

# Weyl-link semimetals

Po-Yao Chang<sup>1,\*</sup> and Chuck-Hou Yee<sup>1,†</sup>

<sup>1</sup>*Center for Materials Theory, Rutgers University, Piscataway, New Jersey, 08854, USA*

A family of topological semimetallic phases where two-fold degenerate gapless points form linked rings is introduced. We refer to this phase as Weyl-link semimetals. A concrete two-band model with two linked nodal lines is constructed. We demonstrate that the Chern-Simons 3-form depends on the linking number of rings in a generic two-band model. In addition, we show the emergence of zero-energy modes in the Landau level spectrum can reveal the location of nodal lines, providing a method of probing their linking number.

## INTRODUCTION

The application of topology to condensed matter physics has produced rich insights into the behavior of an entire class of materials. The integer quantum Hall state, as well as topological insulators and superconductors [1–6], are characterized by the topology of their ground state wave function. These topological structures give rise to protected gapless boundary modes and quantized electromagnetic and gravito-magnetoelectric responses [7, 8]. In addition to fully gapped topological phases, semimetals and nodal superconductors can also exhibit interesting topological properties. Of particular interest are Weyl semimetals [9–11], where the band touching points in the bulk behave as monopoles in momentum space. These monopoles are sources and drains of Berry flux, which leads to anomalous electromagnetic transport and the emergence of surface Fermi arcs. In addition to Weyl semimetals, the set of gapless points in the bandstructure can also form one-dimensional nodal lines and rings [12–15]. These nodal-ring semimetals and superconductors also exhibit robust drumhead surface states [13, 16]. Many material candidates have been proposed and some have been experimentally confirmed [17–27].

In general, the complexity of gapless phases is richer than gapped phases in the following sense: gapped phases are like a featureless vacuum while the point and line nodes in gapless phases behave as defects in momentum space carrying topological charge. As mentioned above, point nodes behave like monopoles of Berry flux, while line nodes are akin to flux tubes (or solenoids). The interplay between these momentum defects often leads to observable effects. For example, nodal points and lines can coexist in the momentum space [28]. Nodal lines can intersect to form states termed nodal-chains [29, 30]. Finally, the line defects can share termination points which can be seen as the momentum space equivalent of the real space nexus previously discussed in helium-3 [31–33].

We extend the family of gapless phases by constructing a minimal two-band model containing two linked nodal rings, with the linking number controlled by an integer  $n$ . We refer to this phase as a Weyl-link semimetal (WLSM). Similar to a nodal-ring semimetal, the non-vanishing Berry phase around the nodal rings in a WLSM leads to drumhead surface states. We show the Chern-Simons 3-form can serve as a topological invariant of the linking number of nodal rings in the two-band

model. In the context of three-dimensional (3D) topological insulators, the  $\theta$ -angle in the axion Lagrangian is related to the Chern-Simons 3-form, where the axion Lagrangian [7] is,

$$\mathcal{S}_\theta^{\text{EM}} = \frac{\theta e^2}{2\pi\hbar c} \int dt d^3x \mathbf{E} \cdot \mathbf{B}. \quad (1)$$

Since the axion Lagrangian can also be present in semimetallic phases such as Weyl semimetals [34–36], the nonvanishing Chern-Simons 3-form in the WLSM potentially may affect magnetoelectric transport. In addition, we analyze the Landau level spectrum in the WLSM and observe the emergence of zero-energy modes. The zero-energy modes in the Landau level spectrum reflect the locations of the nodal rings. Thus, the Landau level spectrum provides a method of probing whether the nodal lines are linked or not, similar to the use of quantum oscillation measurements for mapping out the topology of Fermi surfaces in metals.

## TWO-BAND MODELS AND SURFACE STATES

We construct a two-band model containing two Weyl rings which link an arbitrary number of times by considering the hamiltonian

$$\mathcal{H}(\mathbf{k}) = f(\mathbf{k})\sigma_x + g(\mathbf{k})\sigma_y, \quad (2)$$

where  $\sigma_x$  and  $\sigma_y$  are Pauli matrices. This is a valid hamiltonian for any periodic  $f(\mathbf{k})$  and  $g(\mathbf{k})$  in the Brillouin zone (BZ). The energy spectrum is  $E_\pm(\mathbf{k}) = \pm\sqrt{f^2(\mathbf{k}) + g^2(\mathbf{k})}$  and the corresponding eigenstates are

$$|u_\pm(\mathbf{k})\rangle = \frac{1}{\sqrt{2E_\pm^2(\mathbf{k})}} \begin{pmatrix} \pm f(\mathbf{k}) \mp ig(\mathbf{k}) \\ |E_\pm(\mathbf{k})| \end{pmatrix}. \quad (3)$$

The two bands touch whenever both  $f$  and  $g$  vanish. For a general 3D system, the zeros of these functions form 2D surfaces, and their intersection will form 1D nodal lines in the BZ. For a concrete realization of a WLSM, we choose the following:

$$\begin{aligned} f(\mathbf{k}) &= t(1 + \cos k_x + \cos k_y), \\ g(\mathbf{k}) &= t[\cos(nk_z) + \sin(nk_z)] \sin k_x \\ &\quad + t[\cos(nk_z) - \sin(nk_z)] \sin k_y, \end{aligned} \quad (4)$$

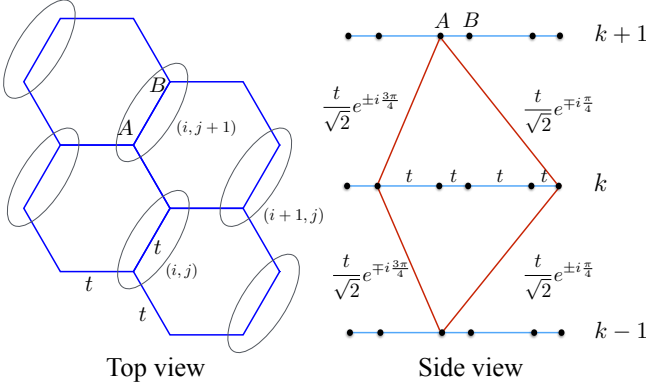


FIG. 1. Tight-binding model for  $n = 1$  case. The top view indicates a graphene like structure with  $A$  and  $B$  sites per unit cell and the hopping amplitude  $t$ . The side view shows the inter-layer hopping with additional phases  $e^{\pm i\pi/4}$  and  $e^{\pm i3\pi/4}$  as described in Eq. (5).

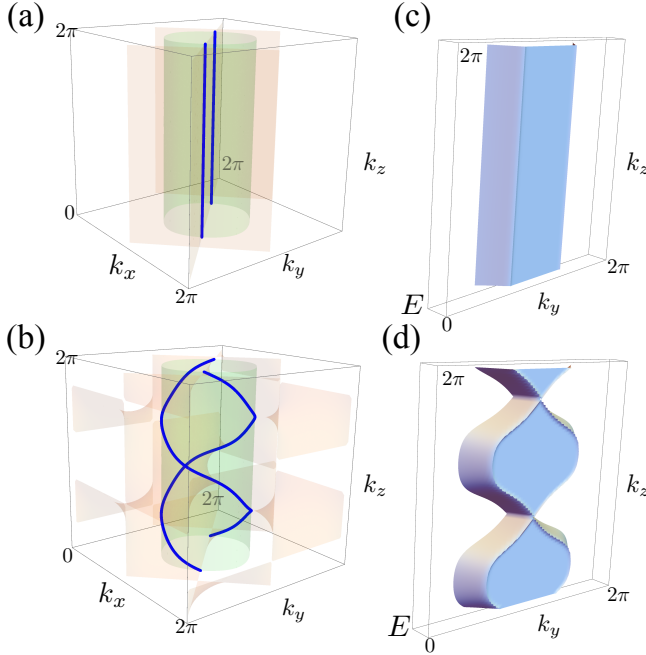


FIG. 2. (a) Weyl-link semimetal (WLSM) with linking number  $n = 0$ . The red and green surfaces are the set of points where  $f(\mathbf{k}) = 0$  and  $g(\mathbf{k}) = 0$  respectively. The nodal lines (blue) are the intersections between these two surfaces. (b) Energy spectrum of the (100) surface states: the flat surface bands are bounded by the projected bulk nodal lines. (c) The WLSM with  $n = 1$ , an example of two linked nodal lines, and (d) its corresponding surface states. The parameter  $t = 1$  for both model in Eq. (4).

The surfaces of zeros of  $f$  and  $g$  intersect and form the desired Weyl links, as shown in Fig. 2. The integer  $n$  determines the (signed) linking number, and negative  $n$  corresponding to the opposite helicity in the  $k_z$  direction. For  $n = \pm 1$ , Weyl rings link once while winding around the BZ, and is topologically equivalent to the Hopf link.

One may worry about the mass term  $m(\mathbf{k})\sigma_z$  and shift

$h(\mathbf{k}) \cdot \mathbb{I}_{2 \times 2}$  present in generic 2-band models. The shift  $h$  is difficult to remove via symmetry constraints, but its presence does not gap out the nodal lines, rather only shifting them in energy. If  $h$  is small relative to the other terms, the nodal lines will broaden to become small Fermi pockets as the nodal line shifts above and below the Fermi level. The mass term  $m(\mathbf{k})\sigma_z$  does gap out the nodal lines, and can be eliminated via symmetry constraints. In the presence of chiral (sublattice) symmetry, the hamiltonian must satisfy  $\mathcal{S}^{-1}\mathcal{H}(\mathbf{k})\mathcal{S} = -\mathcal{H}(\mathbf{k})$  with  $\mathcal{S} = \sigma_3$ , thus forbidding a mass term. The hamiltonian can also be rotated to form  $\tilde{\mathcal{H}}(\mathbf{k}) = f(\mathbf{k})\sigma_x + g(\mathbf{k})\sigma_z$ . In this basis, inversion symmetry combined with time-reversal symmetry ( $\mathcal{PT}$ ) forces the Hamiltonian  $\tilde{\mathcal{H}}(\mathbf{k})$  be real, forbidding the mass term  $m\sigma_y$  and protecting the nodal lines [12, 14, 15].

In principle, there is no symmetry requirement that forces the nodal lines to be linked. However, the physical realization of the model proposed in Eq. (4) is related to the Weyl points in spinless graphene. Let us suppose we monitor the Weyl points in spinless graphene in a rotating frame with the rotation axis perpendicular to the graphene and the rotation angle being  $nk_z$ . The momenta  $(k_x, k_y)$  will be transformed as  $(\cos(nk_z)k_x - \sin(nk_z)k_y, \sin(nk_z)k_x + \cos(nk_z)k_y)$ . In this rotating frame, two Weyl points will form two linked nodal lines along the  $k_z$  direction.

The idea of rotating frame in graphene leads to a concrete tight-binding model in the real space. In the case that the linking parameter vanishes  $n = 0$ , the tight-binding model of Eq. (4) describes the layered graphene with vanishing inter-layer hopping. In the case that the linking parameter  $n = 1$ , the tight-binding model of Eq. (4) in the real space can be written as

$$\begin{aligned}
 H = & t \sum_r c_{r,A}^\dagger c_{r,B} + c_{r+\hat{x},A}^\dagger c_{r,B} + c_{r+\hat{y},A}^\dagger c_{r,B} \\
 & + \frac{1}{\sqrt{2}} (e^{i3\pi/4} c_{r+\hat{x}+\hat{z},A}^\dagger c_{r,B} + e^{-i3\pi/4} c_{r+\hat{x}-\hat{z},A}^\dagger c_{r,B} \\
 & + e^{-i\pi/4} c_{r-\hat{x}+\hat{z},A}^\dagger c_{r,B} + e^{i\pi/4} c_{r-\hat{x}-\hat{z},A}^\dagger c_{r,B} \\
 & + e^{-i3\pi/4} c_{r+\hat{y}+\hat{z},A}^\dagger c_{r,B} + e^{i3\pi/4} c_{r+\hat{y}-\hat{z},A}^\dagger c_{r,B} \\
 & + e^{i\pi/4} c_{r-\hat{y}+\hat{z},A}^\dagger c_{r,B} + e^{-i\pi/4} c_{r-\hat{y}-\hat{z},A}^\dagger c_{r,B}) \\
 & + \text{h.c.}
 \end{aligned} \tag{5}$$

The first three terms describe the hopping between  $A$  and  $B$  sites within the same layer as the tight-binding model for a single graphene sheet. The other terms describe the inter-layer hopping between  $A$  and  $B$  sites as shown in Fig. 1.

The nodal lines behave like vortex tubes in momentum space. The vorticity is the topological charge of the line, and is given by the Berry phase divided by  $2\pi$ ,

$$\nu_\alpha = \frac{1}{2\pi} \oint_{C_\alpha} a, \tag{6}$$

where the Berry connection is

$$a = i\langle u_-(\mathbf{k}) | \partial_{k_i} u_-(\mathbf{k}) \rangle dk_i = \frac{g\partial_{k_i} f - f\partial_{k_i} g}{2(f^2 + g^2)} dk_i, \quad (7)$$

and  $\mathcal{C}_\alpha$  is a loop encircling  $\alpha$ -th nodal line. Since the Berry phase is defined modulo  $2\pi$ , the topological charge of a single nodal line is either  $+1/2$  or  $-1/2$ , depending on the relative orientation of the probing loop  $\mathcal{C}_\alpha$  versus the vorticity direction of the line  $\mathcal{L}_\alpha$ .

Depending on the geometry of the projection of the nodal lines onto the surface BZ, the finite topological charge can lead to flat surface bands [12, 13]. In Fig. 2(b), we plot the spectrum as a function of  $(k_y, k_z)$  for bands on the (100) surface. The flat bands are bounded by the nodal lines projected onto the surface BZ. However, flat bands appear for all linking numbers, including the case  $n = 0$  where the surface states are simply bounded by the two straight nodal lines. Searching for “pinch points” on the surface bands is not sufficient to confirm linked lines, as one can construct unlinked loops with non-planar geometries where pinch points still appear. In the following, we suggest two approaches to probe the linking number of nodal lines. First, we show the Chern-Simons 3-form evaluated over the Brillouin zone is related to the linking number. The Chern-Simons 3-form is related to the axion Lagrangian, a quantity also present in Weyl semimetals. Future work may uncover how linked nodal rings affect the magnetoelectric transport. Second, we compute the Landau level spectrum and show the consequences of linked vs. unlinked nodal lines.

## LINKING NUMBERS AND CHERN-SIMONS THEORY

We are interested in defining a topological invariant that distinguishes whether the rings are linked or not. In the standard effective field theory of 3D topological insulators, the term of interest is the axion Lagrangian Eq. (1) with  $\theta$  constrained by time-reversal symmetry to be either zero or  $\pi$ . The  $\theta$  angle can be computed from the Berry connection via the Chern-Simons 3-form,

$$\theta = \frac{1}{4\pi} \int_{\text{BZ}} \text{Tr}(a \wedge da - \frac{2i}{3} a \wedge a \wedge a). \quad (8)$$

In the case of an abelian Chern-Simons theory, Polyakov and Witten showed that this form is deeply related to the linking number  $N$  of Wilson loops [37]. The linking number is one of the most basic invariants characterizing loops, and is computed using the Gauss linking integral,

$$N(\mathcal{L}_\alpha, \mathcal{L}_\beta) = \frac{1}{4\pi} \oint_{\mathcal{L}_\alpha} dx^i \oint_{\mathcal{L}_\beta} dy^j \epsilon_{ijk} \frac{(x-y)^k}{|x-y|^3}, \quad (9)$$

which determines the (signed) number of times two loops  $\mathcal{L}_\alpha$  and  $\mathcal{L}_\beta$  intertwine with one another. This theory has been

applied to solid state in the context of line-node superconductors, with the line-nodes playing the role of Wilson loops [38]. It is shown that the linking number is related to the Chern-Simons form by

$$\frac{1}{4\pi} \int a \wedge da = \pi \sum_{\alpha, \beta} \nu_\alpha \nu_\beta N(\mathcal{L}_\alpha, \mathcal{L}_\beta), \quad (10)$$

where  $\nu_\alpha$  and  $\nu_\beta$  are the vorticities associated with the nodal rings. We assume the self-linking number  $N(\mathcal{L}_\alpha, \mathcal{L}_\alpha)$  is zero. A heuristic sketch of the above equality is shown in the Supplemental Material [39].

The relationship of the Chern-Simons form to the linking number is rather subtle due to the nodal lines. Consider first the magnetic field  $da$  associated with a nodal line  $\mathcal{L}_\alpha$ . Applying Gauss’ theorem to Eq. (6) gives

$$2\pi\nu_\alpha = \oint_{\mathcal{C}_\alpha} a = \int_{\mathcal{S}_\alpha} da, \quad (11)$$

where  $\mathcal{S}_\alpha$  is the oriented surface bounded by an arbitrary loop  $\mathcal{C}_\alpha$  encircling the nodal line  $\mathcal{L}_\alpha$ . This implies the magnetic field must vanish everywhere except right along the nodal line,

$$da = \sum_{\alpha} 2\pi\nu_\alpha \delta^{(2)}(\mathbf{k}_\perp - \mathcal{L}_\alpha) d\mathbf{k}_\perp^1 \wedge d\mathbf{k}_\perp^2, \quad (12)$$

where  $\delta^{(2)}(\mathbf{k}_\perp - \mathcal{L}_\alpha)$  is the two-dimensional delta function at the nodal line and  $\mathbf{k}_\perp$  is the two component vector lying perpendicular to the direction of  $\mathcal{L}_\alpha$ . Note the sign of the charge  $\nu_\alpha$  depends on the local choice of the coordinate system  $\mathbf{k}_\perp$ . Since the magnetic field is nonzero only along the line node, the integral of the Chern-Simons form over the BZ becomes a line integral of  $\mathcal{L}_\alpha$ :

$$\frac{1}{4\pi} \int_{\text{BZ}} a \wedge da = \frac{1}{2} \sum_{\alpha} \nu_\alpha \oint_{\mathcal{L}_\alpha} a \quad (13)$$

$$= \pi \sum_{\alpha, \beta} \nu_\alpha \nu_\beta N(\mathcal{L}_\alpha, \mathcal{L}_\beta). \quad (14)$$

Strictly, the integral  $\oint_{\mathcal{L}_\alpha} a$ , which encircles the ring  $\mathcal{L}_\beta$ , is undefined since the Berry connection is ill-defined along  $\mathcal{L}_\alpha$ . However, if one allows the integration path to be slightly deformed away from the nodal line via  $\mathcal{L}_\alpha \rightarrow \mathcal{C}_\beta$ , the integral becomes the topological charge of  $\mathcal{L}_\beta$  multiplied by the number of times  $\mathcal{L}_\alpha$  encircles the nodal line  $\mathcal{L}_\beta$ . For the model described by Eq. (4), we have  $\nu_\alpha \nu_\beta = -1/4$ , leading to  $\theta = N\pi/2$ , where  $N$  is the linking number between the two nodal rings. This quantization condition is a result of chiral symmetry: in Weyl-link semimetals, the Chern-Simons 3-form is reduced to the Chern-Simons 1-form because the two-dimensional delta functions along the nodal lines reduces the integral over the Brillouin zone to line integrals. In the presence of chiral symmetry, the Chern-Simons 1-form is quantized [6]. Combined with the  $\pm 1/2$  topological charge of the nodal lines, Chern-Simons 3-form is quantized as  $\theta = N\pi/2$ .

In two-band models, the non-vanishing linking number derived from  $\int ada$  arises from the divergent behavior of the

Berry connection  $a$  at the nodal lines. In the presence of finite mass term  $m\sigma_z$ , the Berry connection and Berry curvature are well-defined in the entire BZ,

$$a = \frac{g\partial_{k_i}f - f\partial_{k_i}g}{2\xi(\xi + m)}dk_i, \quad (15)$$

$$da = -\frac{m}{\xi^3}(\partial_{k_j}f\partial_{k_k}g)dk_j \wedge dk_k, \quad (16)$$

where  $\xi = \sqrt{f^2 + g^2 + m^2}$ . One can directly compute  $\int ada$  unambiguously and the integral uniformly vanishes since  $a$  and  $da$  are perpendicular to each other. Mathematically, it can be shown that for a well-defined Berry connection  $a$ , at least four bands are necessary for a finite value of  $\int ada$ .

A model with two linked Weyl rings need not have a nonzero Chern-Simons 3-form because the two rings may originate from decoupled blocks of the hamiltonian. Specifically, we consider a minimal four-band model

$$\mathcal{H}(\mathbf{k}) = \begin{pmatrix} \mathcal{H}_1(\mathbf{k}) & \\ & \mathcal{H}_2(\mathbf{k}) \end{pmatrix}, \quad (17)$$

where  $\mathcal{H}_1(\mathbf{k})$  produces the set of rings  $\{\mathcal{L}_\alpha^1\}$  and  $\mathcal{H}_2(\mathbf{k})$  similarly produces  $\{\mathcal{L}_\alpha^2\}$ . The Berry connection over the filled bands  $a_{\alpha\beta}$  is a diagonal  $2 \times 2$  matrix with elements  $a_{\alpha\alpha} = \langle u_\alpha^- | \partial u_\alpha^- \rangle dk_i$  on the diagonal. Here,  $|u_\alpha^- \rangle$  is the occupied band for  $\mathcal{H}_\alpha(\mathbf{k})$ ,  $\alpha = 1, 2$ . The Chern-Simons form then decomposes into a simple sum

$$\int \text{Tr}(ada) = \int a_{11}da_{11} + \int a_{22}da_{22}. \quad (18)$$

Even though the two sets of rings  $\{\mathcal{L}_\alpha^1\}$  and  $\{\mathcal{L}_\beta^1\}$  may be linked in the BZ, the links across the two sets do not contribute to the Chern-Simons 3-form. Thus, there can be trivial WLSMs with  $\theta = 0$ .

In 3D topological insulators, the  $\theta$ -term in the axion Lagrangian plays an essential role in their response to electromagnetic fields. In gapped phases, the derivation of the axion Lagrangian is a well-defined procedure: integrate out the fermions to leave a low energy theory in terms of the physical electromagnetic gauge field. In gapless phases, fermions

coexist with the gauge field at the nodal points and lines, so their response may not be separable from the topological effects of the axion Lagrangian. Nevertheless, the  $\theta$ -term has been computed in Weyl semimetals via integration of the fermions [34]. We propose that a similar procedure may be fruitful for WLSM and may relate the linking number of the nodal lines to transport.

## LANDAU LEVEL SPECTRUM

The Landau level spectrum provides an independent probe of the linking of nodal rings. Consider the continuous version of the model in Eq. (2), derived by expanding the functions  $f$  and  $g$  up to second order in momentum:

$$f(\mathbf{k}) \rightarrow 3 - \frac{1}{2}(k_x^2 + k_y^2) \quad (19)$$

$$g(\mathbf{k}) \rightarrow \left(1 - \frac{1}{2}(nk_z)^2 + nk_z\right)k_x + \left(1 - \frac{1}{2}(nk_z)^2 - nk_z\right)k_y. \quad (20)$$

For the specific case when the magnetic field lies along the  $z$ -direction, we do not expand the  $k_z$  terms, keeping them as  $\cos nk_z$  and  $\sin nk_z$ . In the presence of the magnetic field  $B_\gamma$  along  $\gamma$ -direction ( $\gamma = x, y, z$ ), the momentum  $k_\gamma$  is a good quantum number and the Hamiltonian can be parametrized as  $\mathcal{H}(k_\gamma, B_\gamma)$ . By introducing the ladder operators  $a$  and  $a^\dagger$ , we can write the conjugate momenta as  $\Pi_\alpha = k_\alpha - eA_\alpha = \frac{1}{\sqrt{2}l_B}(a^\dagger + a)$  and  $\Pi_\beta = k_\beta - eA_\beta = \frac{1}{\sqrt{2}il_B}(a^\dagger - a)$  with  $l_B = 1/\sqrt{eB_\gamma}$  being the magnetic length. Here,  $(\alpha, \beta, \gamma)$  form a cyclic permutation of  $(x, y, z)$ . The Hamiltonian is a two by two matrix with parameters  $(k_\gamma, B_\gamma)$  and ladder operators  $(a, a^\dagger)$ . The eigenfunction satisfies  $\mathcal{H}(k_\gamma, B_\gamma)\Psi = E(k_\gamma, B_\gamma)\Psi$ , with  $\Psi = (\sum_m \alpha_m |m\rangle, \sum_m \beta_m |m\rangle)^T$ , where  $|m\rangle$  is the state that satisfies  $a^\dagger |m\rangle = \sqrt{m+1} |m+1\rangle$  and  $a |m\rangle = \sqrt{m} |m-1\rangle$ .

---

The Landau level spectrum can be obtained by solving coupled equations of the form

$$\begin{aligned} \mathbb{A}_m \beta_{m+3} + \mathbb{B}_m \beta_{m+2} + \mathbb{C}_m \beta_{m+1} + \mathbb{D}_m \beta_m + \mathbb{E}_m \beta_{m-1} + \mathbb{F}_m \beta_{m-2} + \mathbb{G}_m \beta_{m-3} &= E(k_\gamma, B_\gamma) \alpha_m, \\ \mathbb{G}_{m+3}^* \alpha_{m+3} + \mathbb{F}_{m+2}^* \alpha_{m+2} + \mathbb{E}_{m+1}^* \alpha_{m+1} + \mathbb{D}_m^* \alpha_m + \mathbb{C}_{m-1}^* \alpha_{m-1} + \mathbb{B}_{m-2}^* \alpha_{m-2} + \mathbb{A}_{m-3}^* \alpha_{m-3} &= E(k_\gamma, B_\gamma) \beta_m, \end{aligned} \quad (21)$$

where  $m \geq 0$  and  $\mathbb{A}_n, \mathbb{B}_n, \mathbb{C}_n, \mathbb{D}_n, \mathbb{E}_n, \mathbb{F}_n$ , and  $\mathbb{G}_n$  are the coefficients depend on the direction of the magnetic field (see Supplemental Material [39]).

For a magnetic field oriented along the  $z$ -direction, the Landau level spectrum is dispersionless as a function of  $k_z$  and independent of the linking parameter  $n$ . As shown in Fig. 3(a), the level spacing is proportional to  $\sqrt{m}$ , where  $m$  is the Lan-

---

dau level index. At each fixed  $k_z$  slice, the system is effectively a two-dimensional spinless graphene sheet with two Weyl points which give rise to the doubly degenerate Landau level spectrum  $E_m = \text{sgn}(m)eB_z\sqrt{|m|}$ . Since the distance



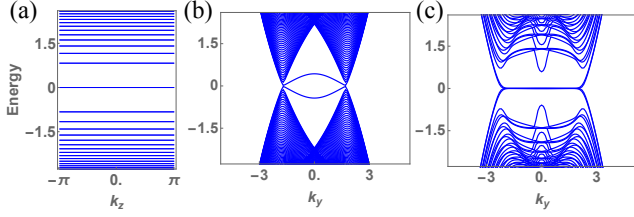


FIG. 3. The Landau level spectra as a function of momentum. (a) The magnetic field along  $z$ -direction with arbitrary linking parameter  $n$ , (b) the magnetic field along  $y$ -direction with linking parameter  $n = 0$  and (c) the magnetic field along  $y$ -direction with linking parameter  $n = 1$ .

between the two Weyl points in the  $k_x$ - $k_y$  plane is the same for any linking parameter  $n$ , the Landau level spectrum is independent of the linking parameter  $n$ .

For a magnetic field oriented along the  $y$ -direction, the Landau level spectrum strongly depends on the linking parameter  $n$ . For unlinked lines ( $n = 0$ ), the Landau level spectrum  $E_m(k_y)$  closes at the nodal lines locations projected on  $k_y$  axis. In between these two gap closing points, there are two dispersive mid-gap states, as shown in Fig. 3(b). For linked lines ( $n = 1$ ), the Landau level spectrum has four dispersionless zero-energy modes in between the two gap closing points [Fig. 3(c)]. This four-fold degeneracy originates from the four Weyl points that pierce each fixed  $k_y$  slice that lies between the two gap closing points, and each Weyl point contributes one zero mode. These zero modes are stabilized by chiral symmetry. By changing the orientation of the magnetic field, the location of the nodal lines can be mapped out and their linking number determined, similar to the use of quantum oscillation measurements for mapping out Fermi surface geometry.

## CONCLUSION AND OUTLOOK

We introduce a two-band model that generates a family of WLSMs with arbitrary linking number. We show that the linking number of the nodal rings is related to the Chern-Simons 3-form. One possible materials candidate is a 3D carbon allotrope composed of pentagonal rings proposed by Zhong, *et.al.*, [40]. The electronic structure of the 3D carbon allotrope under strain exhibits a Weyl-link semimetallic phase. We note that the minimal model for the 3D carbon allotrope is a three-band model, where the two nodal rings originate from the crossing of two different pairs of bands. In the future, we hope to apply this construction based on the intersection of two hypersurfaces to produce semimetals with trefoil knots [41].

## NOTE ADDED

During the preparation of this manuscript, we became aware of related work by Chen, *et.al.* [42] and Yan, *et. al.* [43].

## ACKNOWLEDGEMENTS

The authors would like to thank Yuanping Chen, Elio König, Piers Coleman and David Vanderbilt for valuable discussions. P.-Y. C. was supported by the Rutgers Center for Materials Theory postdoctoral grant. C.H.Y. was supported in part by the Center for Emergent Superconductivity, an Energy Frontier Research Center funded by the US Department of Energy, Office of Science, Office of Basic Energy Sciences under Award No. DEAC0298CH1088.

\* [pychang@physics.rutgers.edu](mailto:pychang@physics.rutgers.edu)

† [chuckyee@physics.rutgers.edu](mailto:chuckyee@physics.rutgers.edu)

- [1] M. König, S. Wiedmann, C. Brüne, A. Roth, H. Buhmann, L. W. Molenkamp, X.-L. Qi, and S.-C. Zhang, *Science* **318**, 766 (2007).
- [2] D. Hsieh, D. Qian, L. Wray, Y. Xia, Y. S. Hor, R. J. Cava, and M. Z. Hasan, *Nature* **452**, 970 (2008).
- [3] M. Z. Hasan and C. L. Kane, *Rev. Mod. Phys.* **82**, 3045 (2010).
- [4] X.-L. Qi and S.-C. Zhang, *Rev. Mod. Phys.* **83**, 1057 (2011).
- [5] M. Z. Hasan and J. E. Moore, *Annu. Rev. Condens. Matter Phys.* **2**, 55 (2011).
- [6] S. Ryu, A. P. Schnyder, A. Furusaki, and A. W. W. Ludwig, *New J. Phys.* **12**, 065010 (2010).
- [7] X.-L. Qi, T. L. Hughes, and S.-C. Zhang, *Phys. Rev. B* **78**, 195424 (2008).
- [8] K. Nomura, S. Ryu, A. Furusaki, and N. Nagaosa, *Phys. Rev. Lett.* **108**, 026802 (2012).
- [9] H. Weng, C. Fang, Z. Fang, B. A. Bernevig, and X. Dai, *Phys. Rev. X* **5**, 011029 (2015).
- [10] J. Liu and D. Vanderbilt, *Phys. Rev. B* **90**, 155316 (2014).
- [11] S.-Y. Xu, I. Belopolski, N. Alidoust, M. Neupane, C. Zhang, R. Sankar, S.-M. Huang, C.-C. Lee, G. Chang, B. Wang, G. Bian, H. Zheng, D. S. Sanchez, F. Chou, H. Lin, S. Jia, and M. Zahid Hasan, arXiv:1502.03807 (2015).
- [12] A. A. Burkov, M. D. Hook, and L. Balents, *Phys. Rev. B* **84**, 235126 (2011).
- [13] S. Matsuura, P.-Y. Chang, A. P. Schnyder, and S. Ryu, *New Journal of Physics* **15**, 065001 (2013), arXiv:1212.2673 [cond-mat.supr-con].
- [14] C. Fang, Y. Chen, H.-Y. Kee, and L. Fu, *Phys. Rev. B* **92**, 081201 (2015).
- [15] Y. X. Zhao and Y. Lu, *Phys. Rev. Lett.* **118**, 056401 (2017).
- [16] G. Bian, T.-R. Chang, H. Zheng, S. Velury, S.-Y. Xu, T. Neupert, C.-K. Chiu, S.-M. Huang, D. S. Sanchez, I. Belopolski, N. Alidoust, P.-J. Chen, G. Chang, A. Bansil, H.-T. Jeng, H. Lin, and M. Z. Hasan, *Phys. Rev. B* **93**, 121113 (2016), arXiv:1508.07521 [cond-mat.mes-hall].
- [17] R. Yu, H. Weng, Z. Fang, X. Dai, and X. Hu, *Phys. Rev. Lett.* **115**, 036807 (2015).
- [18] Y. Kim, B. J. Wieder, C. L. Kane, and A. M. Rappe, *Phys. Rev. Lett.* **115**, 036806 (2015).
- [19] G. Bian, T.-R. Chang, R. Sankar, S.-Y. Xu, H. Zheng, T. Neupert, C.-K. Chiu, S.-M. Huang, G. Chang, I. Belopolski, D. S. Sanchez, M. Neupane, N. Alidoust, C. Liu, B. Wang, C.-C. Lee, H.-T. Jeng, C. Zhang, Z. Yuan, S. Jia, A. Bansil, F. Chou, H. Lin, and M. Z. Hasan, *Nature Communications* **7**, 10556 (2016).

- [20] Q. Xu, R. Yu, Z. Fang, X. Dai, and H. Weng, *Phys. Rev. B* **95**, 045136 (2017).
- [21] J. L. Lu, W. Luo, X. Y. Li, S. Q. Yang, J. X. Cao, X. G. Gong, and H. J. Xiang, ArXiv e-prints (2016), [arXiv:1603.04596 \[cond-mat.mtrl-sci\]](#).
- [22] J. Hu, Z. Tang, J. Liu, X. Liu, Y. Zhu, D. Graf, K. Myhro, S. Tran, C. N. Lau, J. Wei, and Z. Mao, *Phys. Rev. Lett.* **117**, 016602 (2016).
- [23] L. M. Schoop, M. N. Ali, C. Straßer, A. Topp, A. Varykhalov, D. Marchenko, V. Duppel, S. S. P. Parkin, B. V. Lotsch, and C. R. Ast, *Nature Communications* **7**, 11696 (2016), [arXiv:1509.00861 \[cond-mat.mtrl-sci\]](#).
- [24] R. Singha, A. Pariari, B. Satpati, and P. Mandal, ArXiv e-prints (2016), [arXiv:1602.01993 \[cond-mat.mtrl-sci\]](#).
- [25] C. Chen, X. Xu, J. Jiang, S.-C. Wu, Y. P. Qi, L. X. Yang, M. X. Wang, Y. Sun, N. B. M. Schröter, H. F. Yang, L. M. Schoop, Y. Y. Lv, J. Zhou, Y. B. Chen, S. H. Yao, M. H. Lu, Y. F. Chen, C. Felser, B. H. Yan, Z. K. Liu, and Y. L. Chen, *Phys. Rev. B* **95**, 125126 (2017).
- [26] X. Wang, X. Pan, M. Gao, J. Yu, J. Jiang, J. Zhang, H. Zuo, M. Zhang, Z. Wei, W. Niu, Z. Xia, X. Wan, Y. Chen, F. Song, Y. Xu, B. Wang, G. Wang, and R. Zhang, ArXiv e-prints (2016), [arXiv:1604.00108 \[cond-mat.mtrl-sci\]](#).
- [27] M. Neupane, I. Belopolski, M. M. Hosen, D. S. Sanchez, R. Sankar, M. Szlawaska, S.-Y. Xu, K. Dimitri, N. Dhakal, P. Maldonado, P. M. Oppeneer, D. Kaczorowski, F. Chou, M. Z. Hasan, and T. Durakiewicz, *Phys. Rev. B* **93**, 201104 (2016).
- [28] P. Goswami and A. H. Nevidomskyy, *Phys. Rev. B* **92**, 214504 (2015).
- [29] T. Bzdušek, Q. Wu, A. Rüegg, M. Sigrist, and A. A. Soluyanov, *Nature (London)* **538**, 75 (2016), [arXiv:1604.03112 \[cond-mat.mes-hall\]](#).
- [30] R. Yu, Q. Wu, Z. Fang, and H. Weng, ArXiv e-prints (2017), [arXiv:1701.08502 \[cond-mat.mtrl-sci\]](#).
- [31] T. Hyart and T. T. Heikkilä, *Phys. Rev. B* **93**, 235147 (2016).
- [32] T. T. Heikkilä and G. E. Volovik, *New Journal of Physics* **17**, 093019 (2015), [arXiv:1505.03277 \[cond-mat.mes-hall\]](#).
- [33] Y. Chen et al, unpublished.
- [34] Y. Chen, S. Wu, and A. A. Burkov, *Phys. Rev. B* **88**, 125105 (2013).
- [35] D. T. Son and B. Z. Spivak, *Phys. Rev. B* **88**, 104412 (2013).
- [36] K. Landsteiner, *Phys. Rev. B* **89**, 075124 (2014).
- [37] E. Witten, *Commun. Math. Phys* **121**, 351 (1989).
- [38] B. Lian, C. Vafa, F. Vafa, and S.-C. Zhang, *Phys. Rev. B* **95**, 094512 (2017).
- [39] See Supplemental Material for a heuristic sketch of the relation between the Chern-Simons 3-form and the linking number, and the detail calculation of the Landau level spectrum.
- [40] C. Zhong, Y. Chen, Z.-M. Yu, Y. Xie, H. Wang, S. A. Yang, and S. Zhang, *Nat. Comm.* **8**, 15641 EP (2017).
- [41] P.-Y. Chang and C.-H. Yee, unpublished.
- [42] W. Chen, H.-Z. Lu, and J.-M. Hou, *Phys. Rev. B* **96**, 041102 (2017).
- [43] Z. Yan, R. Bi, H. Shen, L. Lu, S.-C. Zhang, and Z. Wang, *Phys. Rev. B* **96**, 041103 (2017).

## Supplementary Material for “Weyl-link semimetals”.

### Topological invariants for linking number

We demonstrate the relation between the linking number and the Chern-Simons 3-form in Eq. (9) by considering a simple geometry shown in Fig. 4. Let us start with a Hamiltonian,  $\mathcal{H} = k_1\sigma_1 + k_2\sigma_2 + m\sigma_3$ . When the mass term vanishes, the model exhibits a nodal line along  $k_3$  direction. The occupied band is

$$|u^-(\mathbf{k})\rangle = \frac{1}{\sqrt{\xi(\xi+m)}} \begin{pmatrix} -k_1 + ik_2 \\ \xi + m \end{pmatrix}, \quad (22)$$

where  $\xi = \sqrt{k_1^2 + k_2^2 + m^2}$ . Assuming  $m > 0$ , the Berry connection

$$a_1 = \frac{k_2}{2\xi(\xi+m)}, \quad a_2 = \frac{k_1}{2\xi(\xi+m)}, \quad (23)$$

and the Berry curvature

$$f_{12} = \partial_{k_1}a_2 - \partial_{k_2}a_1 = \frac{m}{2\xi^3}. \quad (24)$$

When we take the limit  $m \rightarrow 0$ , the Berry curvature

$$\lim_{m \rightarrow 0} f_{12} = -\pi\delta^{(2)}(k_1, k_2), \quad (25)$$

and the Berry connection in the limit  $m \rightarrow 0$  has only the  $\phi$  component in the cylindrical coordinate

$$a_\phi = -\frac{1}{2k}, \quad k \neq 0 \quad (26)$$

where  $k = \sqrt{k_1^2 + k_2^2}$ .

The topological charge of this nodal line is  $\nu = \frac{1}{2\pi i} \oint a_\phi k d\phi = \frac{1}{2}$ . Now we consider two perpendicular nodal lines separated with distance  $k_0$  as shown in Fig. 4. In Fig. 4(a), one nodal line is encircling the other one, where the dashed lines are at infinite. On the other hand, in Fig. 4(b), these two lines are not linked. We can separate the Berry connection into two  $a = a_1 + a_2$ , where  $a_i$  is the Berry connection generated by  $i$ -th nodal line. We have

$$\int ada = \int (a_1 + a_2)(da_1 + da_2) = \int a_1 da_2 + \int a_2 da_1. \quad (27)$$

Here  $\int a_i da_i = 0$  in the presence of infinitesimal mass term. Let us suppose  $a_1 = -\frac{1}{2k}$  is generated by the nodal line along  $y$  axis and  $da_2 = f_2 = -\pi\delta(k_1)\delta(k_2 + k_0)$  is generated by the nodal line along  $z$  direction at  $(k_x, k_y) = (0, -k_0)$ .

$$\int a_1 da_2 = \frac{\pi}{2k_0} \int dk_3 \frac{k_0^2}{k_0^2 + k_3^2} = \frac{\pi^2}{2}. \quad (28)$$

For the configuration shown in Fig. 4(a),  $\int ada = 4 * \frac{\pi^2}{2} = 2\pi^2$ . From Eq. (9), the Gauss linking number is

$$N(\mathcal{L}_b, \mathcal{L}_c) = \frac{1}{2\pi\nu_b * \nu_c} \frac{1}{4\pi} \int ada = 1, \quad (29)$$

where  $\nu_b = \nu_c = 1/2$ .

On the other hand, for the configuration shown in Fig. 4(b),  $\int ada = 2 * \frac{\pi^2}{2} - 2 * \frac{\pi^2}{2} = 0$ , which indicates the Gauss linking number is zero.

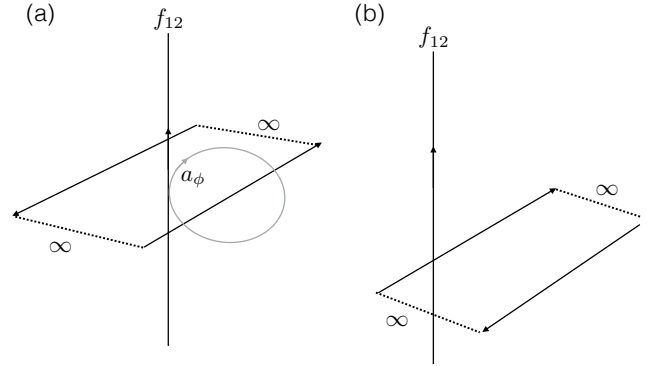


FIG. 4. (a) Linked configuration: one nodal line along  $k_z$  direction and two other nodal lines on the  $k_x - k_y$  plane where they connected at infinity indicated by dashed lines. The vertical nodal line is encircled by the horizontal nodal lines. (b) Unlinked configuration: the vertical nodal line is not encircled by the horizontal nodal lines.

### Landau level spectrum

We consider two orientations of the magnetic field: (a) along  $z$ -direction and (b) along  $y$ -direction. The Hamiltonian in the presence of magnetic field  $B_\gamma$  ( $\gamma = z, y$ ) can be parametrized as  $\mathcal{H}(k_\gamma, B_\gamma)$ . We can introduce the ladder operators  $a$  and  $a^\dagger$  such that the conjugate momenta can be written as  $\Pi_\alpha = k_\alpha - eA_\alpha = \frac{1}{\sqrt{2}l_B}(a^\dagger + a)$  and  $\Pi_\beta = k_\beta - eA_\beta = \frac{1}{\sqrt{2}il_B}(a^\dagger - a)$  with  $l_B = 1/\sqrt{eB_\gamma}$  being the magnetic length. Here  $\alpha, \beta$  and  $\gamma$  form a cyclic order in  $[x, y, z]$ . We solve the Landau level spectrum by introducing a trial wavefunction  $\Psi = (\sum_m \alpha_m |m\rangle, \sum_m \beta_m |m\rangle)^T$  with  $|m\rangle$  being the state that satisfies  $a^\dagger |m\rangle = \sqrt{m+1} |m+1\rangle$  and  $a |m\rangle = \sqrt{m} |m-1\rangle$ . The eigenfunction satisfies  $\mathcal{H}(k_\gamma, B_\gamma)\Psi = E(k_\gamma, B_\gamma)\Psi$ . In the case that the magnetic field pointing along  $z$ -direction, the Hamiltonian (we expand  $\sin k_{x/y} \rightarrow k_{x/y}$  and  $\cos k_{x/y} \rightarrow 1 - \frac{1}{2}k_{x/y}^2$ ) is

$$\mathcal{H}(k_z, B_z) = \left[ 3 - \frac{eB_z}{2}(2a^\dagger a + 1) \right] \mathbb{I}_{2 \times 2} + \sqrt{eB_z} \begin{pmatrix} 0 & -i[e^{i(nk_z - \frac{\pi}{4})}a^\dagger + e^{-i(nk_z - \frac{\pi}{4})}a] \\ i[e^{-i(nk_z - \frac{\pi}{4})}a + e^{i(nk_z - \frac{\pi}{4})}a^\dagger] & 0 \end{pmatrix}. \quad (30)$$

We solve the spectrum by expressing the trial wavefunction  $\Psi = (\sum_m \alpha_m |m\rangle, \sum_m \beta_m |m\rangle)^T$  with  $|m\rangle$  being the state that satisfies  $a^\dagger |m\rangle = \sqrt{m+1} |m+1\rangle$  and  $a |m\rangle = \sqrt{m} |m-1\rangle$ . We have the following coupled equations

$$\begin{aligned} [3 - \frac{eB_z}{2}(2m+1)]\beta_m - i\sqrt{eB_z}[e^{i(nk_z - \frac{\pi}{4})}\sqrt{m}\beta_{m-1} + e^{-i(nk_z - \frac{\pi}{4})}\sqrt{m+1}\beta_{m+1}] &= E(k_z, B_z)\alpha_m, \\ [3 - \frac{eB_z}{2}(2m+1)]\alpha_m + i\sqrt{eB_z}[e^{i(nk_z - \frac{\pi}{4})}\sqrt{m}\alpha_{m-1} + e^{-i(nk_z - \frac{\pi}{4})}\sqrt{m+1}\alpha_{m+1}] &= E(k_z, B_z)\beta_m. \end{aligned} \quad (31)$$

The coefficients in Eq. (21) in the main text,  $\mathbb{A}_m$ ,  $\mathbb{B}_m$ ,  $\mathbb{F}_m$ , and  $\mathbb{G}_m$  are vanishing and  $\mathbb{C}_m = -i\sqrt{eB_z}e^{-i(nk_z - \frac{\pi}{4})}$ ,  $\mathbb{D}_m = 3 - \frac{eB_z}{2}(2m+1)$ ,  $\mathbb{D}_m = -i\sqrt{eB_z}e^{i(nk_z - \frac{\pi}{4})}$ . We observe the spectrum  $E(k_z, B_z)$  is completely flat as a function of  $k_z$  and is independent of  $n$ . These flat bands come from connecting the conventional Landau level in two dimensional Weyl cone on the  $k_z$  slices. Since the Landau level in two dimensional Weyl cones are not sensitive to the location of the cones, the spectrum  $E(k_z, B_z)$  is independent on the linking parameter  $n$ .

In the case that the magnetic field is along  $y$ -direction, the Hamiltonian is

$$\begin{aligned} \mathcal{H}(k_y, B_y) &= \left[ 3 - \frac{1}{2}k_y^2 - \frac{eB_y}{4}(2a^\dagger a + 1) \right] \mathbb{I}_{2 \times 2} + k_y \left[ 1 - \frac{n^2 eB_y}{4}(2a^\dagger a + 1) \right] \sigma_y \\ &+ \frac{eB_y}{4}(1 - 2n) \begin{pmatrix} 0 & a^\dagger a^\dagger \\ aa & 0 \end{pmatrix} + \frac{n^2 k_y eB_y}{4} \begin{pmatrix} 0 & ia^\dagger a^\dagger \\ -iaa & 0 \end{pmatrix} \\ &+ \sqrt{\frac{eB_y}{2}} \left[ (-1 + \frac{n^2 eB_y}{4}) \begin{pmatrix} 0 & a^\dagger \\ a & 0 \end{pmatrix} + nk_y \begin{pmatrix} 0 & ia^\dagger \\ -ia & 0 \end{pmatrix} + \frac{n^2 eB_y}{4} \begin{pmatrix} 0 & a^\dagger a^\dagger a \\ a^\dagger aa & 0 \end{pmatrix} \right] \\ &+ \sqrt{\frac{eB_y}{2}} \left[ (1 - \frac{n^2 eB_y}{4}) \begin{pmatrix} 0 & a \\ a^\dagger & 0 \end{pmatrix} + nk_y \begin{pmatrix} 0 & ia \\ -ia^\dagger & 0 \end{pmatrix} - \frac{n^2 eB_y}{4} \begin{pmatrix} 0 & a^\dagger aa \\ a^\dagger a^\dagger a & 0 \end{pmatrix} \right] \\ &+ \sqrt{\frac{eB_y}{2}} \frac{n^2 eB_y}{4} \begin{pmatrix} 0 & a^\dagger a^\dagger a^\dagger - aaa \\ aaa - a^\dagger a^\dagger a^\dagger & 0 \end{pmatrix}. \end{aligned} \quad (32)$$

Here we symmetrize  $\Pi_z^2 \Pi_x \rightarrow \frac{1}{2}[\Pi_z^2 \Pi_x + \Pi_x \Pi_z^2]$ . The coefficients from coupled equations in Eq. (21) in the main text from the trial wavefunction  $\Psi = (\sum_m \alpha_m |m\rangle, \sum_m \beta_m |m\rangle)^T$  with  $|m\rangle$  being the state that satisfies  $a^\dagger |m\rangle = \sqrt{m+1} |m+1\rangle$  and  $a |m\rangle = \sqrt{m} |m-1\rangle$  are

$$\begin{aligned} \mathbb{A}_m &= -\sqrt{\frac{eB_y}{2}} \frac{n^2 eB_y}{4} \sqrt{(m+1)(m+2)(m+3)}, \\ \mathbb{B}_m &= \frac{eB_y}{4}(1 + 2n + in^2 k_y) \sqrt{(m+1)(m+2)}, \\ \mathbb{C}_m &= \sqrt{\frac{eB_y}{2}} \left[ 1 + ink_y - \frac{n^2 eB_y}{4}(1+m) \right] \sqrt{(m+1)}, \\ \mathbb{D}_m &= 3 - \frac{1}{2}k_y^2 - \frac{eB_y}{4}(2m+1) - ik_y \left[ 1 - \frac{n^2 eB_y}{4}(2m+1) \right], \\ \mathbb{E}_m &= \sqrt{\frac{eB_y}{2}} \left[ -1 + ink_y + \frac{n^2 eB_y}{4}m \right] \sqrt{m}, \\ \mathbb{F}_m &= \frac{eB_y}{4}(1 - 2n + in^2 k_y) \sqrt{m(m-1)}, \\ \mathbb{G}_m &= \sqrt{\frac{eB_y}{2}} \frac{n^2 eB_y}{4} \sqrt{m(m-1)(m-2)}. \end{aligned} \quad (33)$$

In the case that the linking parameter  $n = 0$ , the Landau level spectrum  $E_m(k_y)$  has two gap closing points where two nodal lines are located at. On the other hand, in the case that the linking parameter  $n = 1$ , there are four zero-energy modes in the



Landau spectrum  $E_m(k_y)$ . The existence of zero-energy modes are originated from the zero-energy Landau level of Weyl points at a fixed  $k_y$  slide.

